

Dynamical multistability in high-finesse micromechanical optical cavities

Florian Marquardt, J. G. E. Harris and S. M. Girvin

Departments of Physics and Applied Physics, Yale University, PO Box 208284, New Haven, CT 06520 (USA)

We analyze the nonlinear dynamics of a high-finesse optical cavity in which one mirror is mounted on a flexible mechanical element. We find that this system is governed by an array of dynamical attractors, which arise from phase-locking between the mechanical oscillations of the mirror and the ringing of the light intensity in the cavity. We describe an analytical approximation to map out the diagram of attractors in parameter space, derive the slow amplitude dynamics of the system, including thermally activated hopping between different attractors, and suggest a scheme for exploiting the dynamical multistability in the measurement of small displacements.

PACS numbers: 07.10.Cm, 42.79.Gn, 05.45.-a

Introduction. - The radiation pressure exerted by light stored in an optical cavity couples the mechanical degrees of freedom of the cavity mirrors to the optical field. The dynamics which result from this coupling offer novel means for manipulating both the light and the mirrors themselves, for example by generating squeezed [1] or entangled states of light [2] or matter [3], or by tailoring the mechanical properties of the mirrors [4, 5, 6, 7, 8]. The radiation pressure also sets fundamental and practical limits on the sensitivity of a range of experiments, from the km-scale optical cavities in gravitational wave observatories such as LIGO to the μm -scale cavities used to probe the motion of micromechanical systems, e.g. by enforcing the standard quantum limit for displacement measurements [9, 10, 11, 12] or introducing mechanical instabilities [1, 13, 14, 15].

To date the theoretical description of these systems has been almost entirely in terms of linearized equations of motion, valid for small mirror oscillations. While this approach has been adequate to predict a wide range of novel effects, it neglects the inherent nonlinearity of these devices and cannot describe their behavior in dynamically unstable regimes. As advances in micromachining [16, 17, 18, 19] and optical cavity fabrication [20, 21] produce devices with stronger optomechanical coupling and weaker damping than was previously possible, the nonlinearities and dynamical instabilities of these systems will become increasingly important. Here we present an analytic theory which provides a full description of the nonlinear regime. We find that the dynamics is dominated by an array of stable dynamical attractors which correspond to phase-locking between the mirror motion and the ringing in the cavity optical field. These results are confirmed in detail by numerical simulations of the microscopic equations of motion. The theory presented here also describes the statistical behavior of the cantilever oscillation amplitude and thermally-activated transitions between the dynamical attractors.

The model. - We consider the setup of Fig. 1. The coupling between the cantilever position and the light intensity of a given cavity mode is described by the Hamiltonian $\hat{H}_{\text{cav}} = \hbar\omega_L(1 - \hat{x}/l)\hat{a}^\dagger\hat{a}$, provided we may neglect

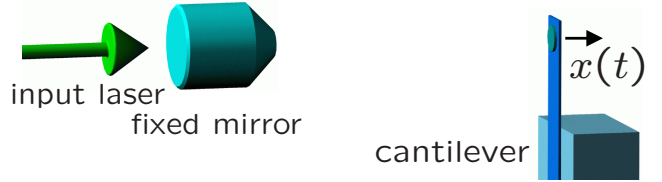


Figure 1: The setup analyzed in the text (not drawn to scale).

the finite travel-time of the light between the mirrors. The cavity of length l is resonant with the incoming laser radiation of frequency ω_L when $x = 0$, and we assume the excursions in x to be small enough to avoid the other resonances. This coupling gives rise to a radiation pressure force $\hat{F} = (\hbar\omega_L/l)\hat{a}^\dagger\hat{a}$. In the following we will consider the purely classical nonlinear dynamics, where \hat{a} is replaced by the coherent light amplitude α . We use the ring-down time of the cavity γ^{-1} , the resonance width $\delta x = l\gamma/\omega_L$, and the cantilever mass m as convenient new units, and rescale α such that it becomes 1 at resonance: $\alpha = \alpha^{\text{orig}} e^{i\omega_L t} / \sqrt{n_{\text{max}}}$, where the maximum photon number $n_{\text{max}} = 4P_{\text{in}}/(\gamma\hbar\omega_L)$ is linear in the input power P_{in} . Then the coupled equations of motion for α and x read [1]:

$$\dot{\alpha} = \left(ix - \frac{1}{2} \right) \alpha + \frac{1}{2} \quad (1)$$

$$\ddot{x} = \mathcal{P}|\alpha|^2 - \omega_0^2(x - x_0) - \Gamma\dot{x} \quad (2)$$

The oscillator frequency ω_0 and mechanical damping rate Γ are fixed, while the detuning from resonance x_0 may be controlled, either by changing the laser frequency or applying a static force to the cantilever. All the other constants are combined into the dimensionless input power

$$\mathcal{P} = \frac{4P_{\text{in}}\omega_L}{m\gamma^4 l^2} = \frac{\hbar n_{\text{max}}}{m\delta x^2 \gamma}. \quad (3)$$

We emphasize that the scale of the radiation pressure, set by \mathcal{P} , grows with the fourth power of the cavity finesse ($\mathcal{P} \propto \gamma^{-4}$ with $\gamma = (c/2l)\mathcal{T}$, where \mathcal{T} is the mirror

transmission). The nonlinear effects we investigate become important for $\Gamma \ll \mathcal{P}$.

This work is motivated in part by the possibility of using the fabrication process described in [17, 18] to integrate ultrasensitive cantilevers with high-reflectivity dielectric mirrors, and to use these mirrors as part of a high-finesse optical cavity at low temperatures. In [18], cantilevers with spring constants of $\sim 10^{-3}$ N/m and mass 10^{-11} kg were integrated with lithographically-patterned high-quality heterostructures similar in design to high-reflectivity dielectric mirrors. These cantilevers were then used in an optical interferometer with an incident power $P_{\text{in}} \sim 20$ nW at $T \sim 0.3$ K. By making modest adjustments to the dimensions of these devices, it should be possible to realize cantilevers with spring constant ~ 1 N/m, mass $m \sim 10^{-10}$ kg, and mechanical $Q \sim 10^5$ supporting a mirror capable of achieving a cavity finesse of $\pi/\mathcal{T} \sim 10^5$, where $l \sim 10$ cm. Assuming these values, the cavity ringdown rate $\gamma \sim 10^5$ Hz becomes comparable with the cantilever frequency ($\omega_0 \sim 1$ in units of γ), and the dimensionless damping rate $\Gamma \sim 10^{-5}$ is much smaller than $\mathcal{P} \sim 1$. In contrast, our estimate for the recent low-finesse experiment on radiation cooling of a cantilever [8] is roughly $\mathcal{P} \sim 10^{-18} \ll \Gamma$ (both for radiation-pressure and photothermal effects).

The cavity resonance peak $\alpha(x) = 1/(1 - 2ix)$ gives rise to a rounded step-like barrier in the effective static cantilever potential obtained by integrating the right-hand-side (rhs) of Eq. (2),

$$V_{\text{eff}}(x) = \frac{\omega_0^2}{2}(x - x_0)^2 - \frac{\mathcal{P}}{2} \arctan(2x). \quad (4)$$

Depending on the parameters $(\omega_0, x_0, \mathcal{P})$, there are one or two local minima of V_{eff} , opening the possibility of *static* bistability [5, 6]. However, it is known [4] that the time-lag of the radiation pressure force generated by the finite cavity ring-down time γ^{-1} introduces additional damping or anti-damping to the left or right of the barrier, respectively. Here we will focus on the regime where the anti-damping leads to a linear dynamical instability discovered previously [1, 13, 14, 22], such that there is no stable stationary solution $\dot{x} = 0$. Then the system settles into self-sustained oscillations, whose full nonlinear dynamics we explore here.

Dynamics in the unstable regime. - Direct numerical solution of Eqs. (1), (2) reveals that $x(t)$ carries out approximately sinusoidal oscillations at the unperturbed frequency ω_0 ,

$$x(t) \approx \bar{x} + A \cos(\omega_0 t). \quad (5)$$

This fact is essential in allowing us to derive an analytical theory for the nonlinear cantilever dynamics. The light amplitude $\alpha(t)$ develops a more complicated behaviour (Fig. 2). It experiences a sharp rise each time

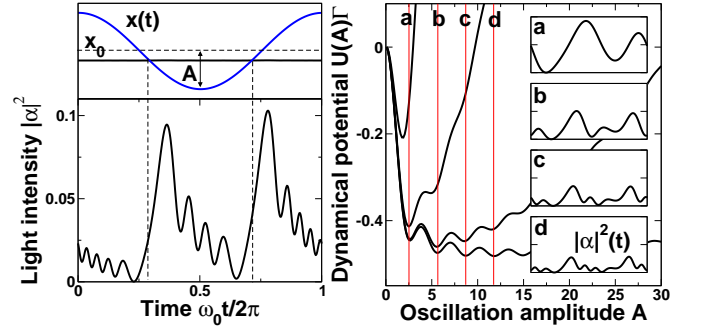


Figure 2: Left: Light intensity oscillations for given sinusoidal cantilever motion (with $\omega_0 = 1$, $\bar{x} = x_0 = 5$, $A = 20$). Right: Resulting dynamical potential $U(A)$, for $\mathcal{P} = 1$ and $\Gamma = 10^{-4}, 10^{-3}, 10^{-2}, 10^{-1}$ (bottom to top curve). Insets show $|\alpha|^2(t)$, with time on the horizontal axis spanning one period and the vertical scale equal to 0.4 in each case. Note the additional oscillation in $|\alpha|^2$ for each subsequent potential well, i.e. each new dynamical attractor.

the cantilever swings through the resonance at $x = 0$. Its dynamics resembles that of a driven damped oscillator which is swept through resonance non-adiabatically. The exact solution for a given $x(t)$ (Eq. (5)) can be written as a Fourier series, $\alpha(t) = e^{i\varphi(t)} \sum_n \alpha_n e^{in\omega_0 t}$, with

$$\alpha_n = \frac{1}{2} \frac{J_n\left(-\frac{A}{\omega_0}\right)}{in\omega_0 + \frac{1}{2} - i\bar{x}}, \quad (6)$$

and a global phase $\varphi(t) = (A/\omega_0) \sin(\omega_0 t)$, where J_n is the Bessel function of the first kind.

Dynamical multistability. - We can determine the possible dynamical attractors (\bar{x}, A) of the cantilever motion by imposing two conditions that follow from Eq. (2) for any periodic motion. The total time-averaged force $\langle \ddot{x} \rangle$ has to vanish, and the net power input via the radiation pressure force must equal the power dissipated through friction, $\langle \dot{x}\ddot{x} \rangle = 0$. This translates into

$$\mathcal{P} \langle |\alpha(t)|^2 \rangle = \omega_0^2 (\bar{x} - x_0) \quad (7)$$

$$P_{\text{rad}} = \mathcal{P} \langle |\alpha(t)|^2 \dot{x} \rangle = P_{\text{fric}} = \Gamma \langle \dot{x}^2 \rangle. \quad (8)$$

The exact dependence on \bar{x}, A and ω_0 follows directly from the coefficients of Eq. (6):

$$\langle |\alpha|^2 \rangle = \sum_n |\alpha_n|^2 \quad (9)$$

$$\tilde{P}_{\text{rad}} = \langle |\alpha|^2 \dot{x} \rangle = A\omega_0 \text{Im} \sum_n \alpha_n^* \alpha_{n+1} \quad (10)$$

The power balance equation can be recast into the form

$$\frac{\tilde{P}_{\text{rad}}(\bar{x}, A)}{\tilde{P}_{\text{fric}}(A)} = \frac{\Gamma}{\mathcal{P}}, \quad (11)$$

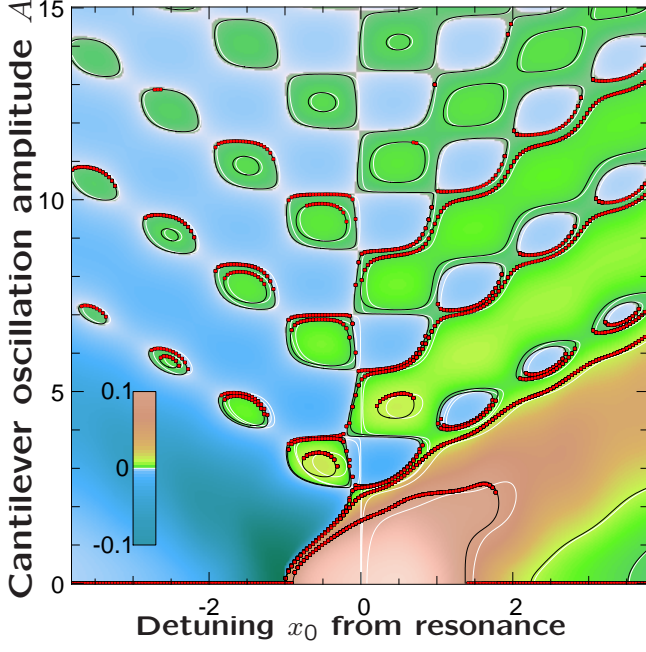


Figure 3: Density plot of the ratio of reduced radiation power input and frictional power loss, $\tilde{P}_{\text{rad}}(\bar{x}(x_0, A), A)/\tilde{P}_{\text{fric}}(A)$, in the (x_0, A) -plane. The contour lines indicate dynamically stable cantilever oscillation amplitudes A , according to Eq. (11). White contour lines display the approximation $\bar{x} \approx x_0$. Contours are drawn for $\Gamma/\mathcal{P} = 10^{-4}, 10^{-3}, 10^{-2}, 10^{-1}$ (with $\mathcal{P} = \omega_0 = 1$). Red dots show the long-time limit ($t_{\text{sim}} = 2 \cdot 10^4$) of the amplitude $A = x_{\text{max}} - x_{\text{min}}$ in the numerically exact solution of the original equations of motion, obtained for the same values of Γ/\mathcal{P} and a set of random initial conditions.

with $\tilde{P}_{\text{fric}}(A) = \omega_0^2 A^2/2$. Stable attractors are those where the ratio decreases for increasing A .

After solving the force balance equation (7) for $\bar{x} = \bar{x}(x_0, A)$, we can plot the contour lines of the lhs of Eq. (11) in the (x_0, A) -plane. These trace out the diagram of possible equilibrium values of the cantilever oscillation amplitude A as a function of detuning x_0 (Fig. 3). The red dots in Fig. 3 show the results of a (much more time-consuming) full simulation of the initial equations of motion, Eqs. (1),(2), confirming that our analytical approximation works extremely well.

The initial onset of the instability at some threshold $x_0^* < 0$ (with $x_0^* = -1$ in Fig. 3) can be described by expanding Eq. (7) for small A (and $\bar{x} \approx 0$), which is valid in the limit $\Gamma \ll \mathcal{P}$. This leads to $A \approx [(1 + 4\omega_0^2)(1 + \omega_0^2 x_0/\mathcal{P})/2]^{1/2}$. The position of the onset, $x_0^* = -\mathcal{P}/\omega_0^2$, and the rise of A do not depend on Γ in this limit.

Near the onset we have $|\bar{x}| \ll x_0$. However, for the rest of parameter space (x_0, A) , we find that $\bar{x} \approx x_0$ is a good approximation (this approximation is shown as the white lines in Fig. 3, as compared to the black lines), becoming exact for $\mathcal{P} \rightarrow 0$. Within this approximation, which we will adopt in the following, we only need to fulfill the

power balance equation (8). Its lhs does not depend on the damping Γ or the dimensionless light power \mathcal{P} , and therefore the equilibrium values of A , at a given x_0 , depend only on the ratio Γ/\mathcal{P} within this approximation.

At large A/ω_0 , we find

$$\tilde{P}_{\text{rad}} \approx \frac{-\omega_0}{2(1 + \omega_0^2)} \cos(2\frac{A}{\omega_0}) \text{Im} \left[\sinh \left(\frac{(\frac{1}{2} - ix_0)\pi}{\omega_0} \right) \right]^{-1}. \quad (12)$$

This reveals explicitly the periodic structure observed in Fig. 3, with periods of $\pi\omega_0$ and $2\omega_0$ in A and x_0 , respectively. Physically, an increase in A enlarges the time-dependent detuning $x(t)$ which is equal to the frequency of the ringing in the light intensity $|\alpha|^2(t)$ (Fig. 2). The appearance of the array of attractors is thus due to a phase-locking phenomenon, where the oscillations of the light intensity (depending on A) seek to be commensurate with the fundamental cantilever period. For the experimental parameters mentioned above, the periods in A and x_0 will be on the picometer scale.

Amplitude equation of motion. - We can determine the slow dynamics of the cantilever oscillation amplitude A by equating the change in total cantilever energy $E = \frac{\omega_0^2}{2}A^2$ to the net power input:

$$\frac{dE}{dt} = P_{\text{total}} = P_{\text{rad}} - P_{\text{fric}} \quad (13)$$

This can be used to obtain the overdamped motion of A ,

$$\frac{dA}{dt} = \frac{1}{A\omega_0^2} P_{\text{total}} = -\frac{\Gamma}{2\omega_0^2} U'(A), \quad (14)$$

where we have introduced the effective potential for A ,

$$U(A) = \frac{\omega_0^2}{2} A^2 - \frac{2\mathcal{P}}{\Gamma} \int_{A_0}^A \tilde{P}_{\text{rad}}(A') \frac{dA'}{A'}. \quad (15)$$

The first part of $U(A)$ is the oscillator potential itself, which drives A towards zero in the absence of radiation pressure ($\mathcal{P} = 0$). The second part produces a decaying oscillating component, as follows from Eq. (12). The total potential $U(A)$, obtained from $\tilde{P}_{\text{rad}}(A)$, in general displays several local minima, corresponding to the dynamical attractors, before the quadratic rise of the first term takes over at large A (see Fig. 2, right). Solving Eq. (14) and comparing to ab-initio simulations of the full dynamics yields a good agreement, which can be improved at small $|x_0|$ by using $\bar{x} = \bar{x}(x_0, A)$ from Eq. (7) instead of $\bar{x} = x_0$. This was also used for Fig. 4.

Stochastic dynamics and Boltzmann distribution. - We can model the stochastic dynamics of this driven nonlinear system within our amplitude equation approach. The heat bath responsible for the intrinsic damping of

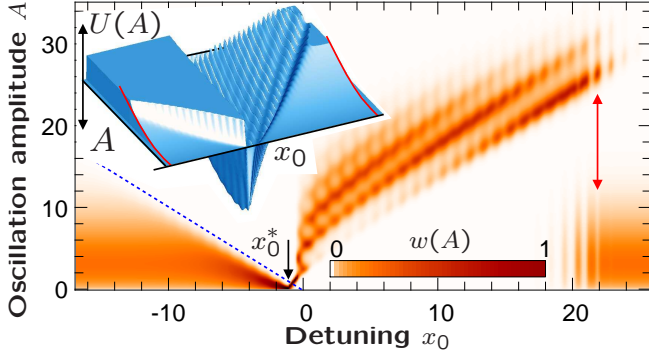


Figure 4: Boltzmann distribution $w(A)$ of the cantilever oscillation amplitude A , as a function of detuning x_0 , for a reduced temperature $\tilde{T} = 10$. Other parameters: $\mathcal{P} = \omega_0 = 1$, $\Gamma = 10^{-3}$. Note the sharp drop in $w(A)$ at $A = -x_0$ (dashed blue line), the narrowing (cooling) of the distribution for $x_0 < 0$, the onset of instability at x_0^* , and the transition(s) above $x_0 = 20$, back to the thermal distribution of an unperturbed oscillator. Inset: Underlying effective potential $U(A)$ (top truncated), with bare oscillator parabolic potential $\omega_0^2 A^2/2$ indicated in red.

the cantilever also produces a fluctuating force, which can be added to the rhs of Eq. (2) as a white-noise term $\xi_X(t)$. The fluctuation-dissipation-theorem demands $\langle \xi_X(t) \xi_X(0) \rangle = 2\Gamma \tilde{T} \delta(t)$, with a reduced temperature $\tilde{T} = k_B T / (m \delta x^2 \gamma^2)$. This gives rise to a fluctuating power $\xi_E = \dot{x} \xi_X$ in Eq. (13), which in turn leads to a stochastic force $\xi_A(t) = \xi_E(t) / (A \omega_0^2)$ on the rhs of the equation of motion (14) for A , with $\langle \xi_A(t) \xi_A(0) \rangle = (\Gamma \tilde{T} / \omega_0^2) \delta(t)$. The cantilever will thus settle into a dynamical, driven equilibrium described by the Boltzmann distribution (Fig. 4)

$$w(A) \propto A \exp \left[-\frac{U(A)}{\tilde{T}} \right]. \quad (16)$$

The prefactor A accounts for the phase space associated with the two quadratures of motion. Formally, it is produced by an additional deterministic term $\Gamma \tilde{T} / (2\omega_0^2 A)$ on the rhs of Eq. (14), which stems from rewriting the Langevin-version of (13) in Ito-form. Comparison with a Langevin-Runge-Kutta [23] simulation of the original Langevin equations for x and α shows good agreement. Shot noise may be neglected for the high photon numbers of interest here ($n_{\max} \sim 10^6$).

As the scale ΔU of the corrugations in the oscillatory “washboard-potential” $U(A)$ is set by the ratio \mathcal{P}/Γ , see Eq. (15), it can become much larger than the light-induced contribution to the static potential V_{eff} , Eq. (4), which scales like \mathcal{P} . Thus, at small intrinsic damping Γ , the dynamically unstable cantilever may display a strong confinement of the oscillation amplitude A in the wells of the dynamical potential, even while radiation effects on the static Boltzmann distribution

$\exp[-V_{\text{eff}}(x)/\tilde{T}]$ would be negligible. In our numerical example, the scale ΔU corresponds to a real temperature in the tens of Kelvin, below which the Boltzmann distribution clearly shows the structure of multiple dynamical attractors. The Kramers rate for thermal hopping between wells is $\tau_{\text{th}}^{-1} = (\Gamma \Delta U / 2\pi \omega_0^4) \exp[-\Delta U/\tilde{T}]$. Both at $x_0 < 0$ and large $x_0 > 0$ the global minimum of $U(A)$ is at $A = 0$, and $w(A)$ returns to the distribution of the unperturbed oscillator.

Photothermal (bolometric) forces can be another source of coupling between light field and cantilever and were used for cooling a cantilever [7, 8]. Due to the finite heat conductance of the cantilever, they feature an additional time-lag τ between light intensity and force, in addition to the time-lag between cantilever motion and intensity already present in the case of radiation pressure. Such a force enters the rhs of the cantilever equation of motion (2) in the form $\mathcal{P}' \tau^{-1} \int_{-\infty}^t dt' |\alpha|^2(t') \exp[-(t-t')/\tau]$, where we have considered the special case $\tau = 0$ up to now. The prefactor \mathcal{P}' is equal to \mathcal{P} multiplied by the ratio between bolometric and radiation pressure force at constant light intensity. The whole preceding analysis still applies, provided we divide the sum in Eq. (10) by the factor $1 + i\omega_0 \tau$ and add up all contributions to P_{rad} and $U(A)$. The oscillatory structure of the potential is fully retained. However, for large $\omega_0 \tau$, the total magnitude of this bolometric contribution is suppressed, such that only the radiation pressure effects remain.

Hysteresis and ‘latching’ measurements. - The presence of multiple locally stable dynamical attractors naturally leads to hysteresis upon sweeping an external parameter. In addition, the sensitivity to parameter perturbations is greatly enhanced near transitions between attractors. This could lend itself to the convenient measurement of very small displacements (i.e. small perturbations δx_0 , on the sub-picometer scale): Sweeping back and forth in x_0 can leave the cantilever in either of two attractors, depending on whether δx_0 was large enough. Afterwards, the resulting (stable) amplitude may be measured. A similar ‘latching’ scheme has been proposed and implemented in a very different context, using the dynamical bistability of a strongly driven Josephson junction [24].

Conclusions. - We have studied the nonlinear classical dynamics of high-finesse micromechanical optical cavities and discovered a form of dynamical multistability that can arise in high-finesse cavities with a large mechanical quality factor of the oscillating mirror. The cantilever undergoes self-sustained oscillations whose amplitude settles into one of several attractors, which we have mapped out in parameter space. We have derived an analytical description of the slow amplitude dynamics, introduced an effective dynamical potential, incorporated the effects of thermal noise leading to tunneling between the potential wells, and extended our analysis to photothermal forces. Finally, we have pointed out that the intrinsic

hysteresis may be useful to implement a ‘latching’ scheme for detecting small displacements. The effects described here should be measurable in cavities that are within the reach of current technology.

Acknowledgments. - We thank J. Gambetta for useful hints on stochastic simulations. F. M. acknowledges support by a DFG scholarship. S. M. G. acknowledges support by NSF-ITR 0325580 and NSF-DMR 0342157.

-
- [1] C. Fabre et al., Phys. Rev. A **49**, 1337 (1994).
 - [2] V. Giovannetti, S. Mancini, and P. Tombesi, Europhysics Letters **54**, 559 (2001).
 - [3] W. Marshall, C. Simon, R. Penrose, and D. Bouwmeester, Phys. Rev. Lett. **91**, 130401 (2003).
 - [4] V. Braginsky and A. Manukin, JETP **25**, 653 (1967).
 - [5] A. Dorsel, J. D. McCullen, P. Meystre, E. Vignes, and H. Walther, Phys. Rev. Lett. **51**, 1550 (1983).
 - [6] P. Meystre, E. M. Wright, J. D. McCullen, and E. Vignes, J. Opt. Soc. Am. B **2**, 1830 (1985).
 - [7] M. Vogel, C. Mooser, K. Karrai, and R. J. Warburton, Applied Physics Letters **83**, 1337 (2003).
 - [8] C. Höhberger-Metzger and K. Karrai, Nature **432**, 1002 (2004).
 - [9] C. M. Caves, Phys. Rev. Lett. **45**, 75 (1980).
 - [10] V. B. Braginsky et al., Phys. Rev. D **57**, 082001 (2003).
 - [11] I. Tittonen et al., Phys. Rev. A **59**, 1038 (1999).
 - [12] J. A. Sidles et al., Rev. Mod. Phys. **67**, 249 (1995).
 - [13] J. M. Aguirregabiria and L. Bel, Phys. Rev. A **36**, 3768 (1987).
 - [14] L. Bel, J. L. Boulanger, and N. Deruelle, Phys. Rev. A **37**, 1563 (1988).
 - [15] V. B. Braginsky, S. E. Strigin, and S. P. Vyatchanin, Physics Letters A **287**, 331 (2001).
 - [16] A. N. Cleland and M. L. Roukes, Nature **392**, 160 (1998).
 - [17] J. G. E. Harris et al., Applied Physics Letters **75**, 1140 (1999).
 - [18] J. G. E. Harris et al., Phys. Rev. Lett. **86**, 4644 (2001).
 - [19] D. Rugar, R. Budakian, H. J. Mamin, and B. W. Chui, Nature **430**, 329 (2004).
 - [20] G. Rempe, R. J. Thompson, H. J. Kimble, and R. Lalezari, Optics Letters **17**, 363 (1992).
 - [21] C. J. Hood, H. J. Kimble, and J. Ye, Phys. Rev. A **64**, 033804 (2001).
 - [22] A. Pai, S. V. Dhurandhar, P. Hello, and J. Y. Vinet, European Physical Journal D **8**, 333 (2000).
 - [23] J. Wilkie, Phys. Rev. E **70**, 017701 (2004).
 - [24] Siddiqi et al., Phys. Rev. Lett. **93**, 207002 (2004) and Phys. Rev. Lett. **94**, 027005 (2005).